# Quantitative Comparison of Bilateral Teleoperation Systems Using $\mu$-Synthesis

Keehoon Kim, *Member, IEEE*, M. Cenk Çavuşoğlu, *Senior Member, IEEE*, and Wan Kyun Chung, *Member, IEEE*

***Abstract*—This paper presents a quantitative comparison framework for bilateral teleoperation systems (BTSs) that have different dynamic characteristics and sensory configurations for a given task-dependent performance objective (TDPO). $\mu$-synthesis is used to develop the framework since it can efficiently treat systems containing uncertainties and disturbances. The framework consists of: 1) a feasibility test and 2) a comparison methodology using prioritized TDPOs. As the formulation used is based on $\mu$-synthesis, the system, operator, and environment models are represented in the form of linear nominal models with frequency-dependent multiplicative uncertainties. This framework is applied to a BTS including an uncertain human operator and environment in a practical case study. The validity of the proposed quantitative framework is confirmed through experiments. The proposed framework can be used as a tool to design BTSs, especially when there are constraints in designing drive mechanisms and choosing sensory configurations.**

***Index Terms*—Bilateral teleoperation system, haptic interface, quantitative comparison, $\mu$-synthesis, task-dependent performance objective.**

## I. Introduction

THE DIFFICULTY in implementing a teleoperation system comes from the unpredictability of human and environment impedances, communication disturbances (i.e., time delay), and quantization error. Previous works in the literature focus on the design of robust controllers to overcome such uncertainties and disturbances from a control point of view. The controllers are designed for a specific master device, slave manipulator, and task. Thus, the teleoperation system with a well-tuned controller can perform the best. This approach is applicable when it is possible for the designer to freely select mechanisms and sensors for the master device and the slave manipulator. However, in most applications, there are constraints in designing mechanisms and choosing sensors, including financial cost. For example, in robotic telesurgical systems for minimally invasive surgery, the size of actuators and the number of sensors are restricted since the slave manipulator works inside the patient through a small port. In such a situation, one has to carefully design drive mechanisms, and distribute the limited number of sensors. In other words, the best architecture implementing a teleoperation system subject to the restrictions of the task should be designed. However, a systematic quantitative methodology comparing different architectures and evaluating design criteria such as dynamic characteristics and sensory configurations is not yet available to guide overall design of teleoperation systems. This paper presents a quantitative comparison (QC) framework for bilateral teleoperation systems (BTSs) that have different dynamic characteristics and sensory configurations for a given task-dependent performance objective (TDPO), in order to provide a framework for the design of BTSs.

The following terms are used through this paper.

1) *BTS*: A system that combines a master device, a slave manipulator, and a controller for transmission of the kinematic and dynamic information.
2) *Task*: The objective of a BTS, such as force and/or position tracking under specified human operator and environment conditions.
3) *TDPO*: The minimal performance specifications of a BTS required to complete the given task, subject to the stability of the BTS.

When determining the design guidelines of a BTS, the human operator, the environment where it is operated, and its objective should be considered. A system can be used in a relatively well-known environment or a very uncertain environment. Sometimes, force-tracking performance is needed rather than position performance or vice versa. Therefore, different design criteria should be applied to design a BTS according to different tasks. In this paper, we define a new term, "TDPO" for quantitative performance specifications of a BTS.

The choice of the performance index is a critical factor for QC. Several different performance indexes have been used in the literature to quantify BTS performance. Hannaford used a two-port network model design framework in which the operator commands position and the interaction force between the slave manipulator and the environment is reflected to the operator [1]. He introduced the hybrid matrix, and discussed how it could be used as a measure of performance of the teleoperator. Anderson and Spong introduced passivity theory and the concept of a scattering matrix to overcome the stability problems resulting from time delay for the two-port interface [2]. The scattering matrix can be used as a measure of the

Manuscript received August 16, 2006; revised February 5, 2007. This paper was recommended for publication by Editor H. Arai and Associate Editor P. Rocco upon evaluation of the reviewer's comments. This work was supported in part by the National Science Foundation, U.S., under Grants CISE IIS-0222743, CISE EIA-0329811, and CISE CNS-0423253, in part by the DoC under Grant TOP-39-60-04003, in part by the Ministry of Health and Welfare, Korea, under Grant 02-PJ3-PG6-EV04–0003, in part by the International Cooperation Research Program (M6-0302-00-0009-03-A01-00-004-00) of the Ministry of Science and Technology, Korea, and in part by the National Research Laboratory (NRL) Program (M1-0302-00-0040-03-J00-00-024-00) of the Ministry of Science and Technology, Korea.

K. Kim is with the Northwestern University, Evanston, IL 60208 USA (e-mail: keehoon-kim@northwestern.edu).

M. C. Çavuşoğlu is with the Case Western Reserve University, Cleveland, OH 44106 USA (e-mail: cavusoglu@case.edu).

W. K. Chung is with Pohang University of Science and Technology (POSTECH), Pohang 790-784, Korea (e-mail: wkchung@postech.ac.kr).

Digital Object Identifier 10.1109/TRO.2007.900625

passivity of the teleoperation system under uncertainty, such as constant time delay. Colgate and Brown suggested the achievable impedance range, $Z$-width, as a measure of performance in sampled data systems [3]. Adams and Hannaford applied virtual coupling to impedance and admittance interfaces so as to find the $Z$-width to satisfy unconditional stability [4]. Lawrence defined transparency as a performance objective matching the environment impedance and the impedance perceived by the human through the teleoperator, and proved that all four information channels are required for high levels of transparency [5]. Yokokohji and Yoshikawa defined a performance index of maneuverability that quantified how well the transfer functions from operator force to master and slave positions and forces match. [6]. Recently, Çavuşoğlu *et al*. suggested a new measure of fidelity that is the sensitivity of the transmitted impedance to changes of the environment impedance. This measure was used to design teleoperation controllers for telesurgical systems [7]. The aforementioned frameworks are based on the assumptions that the operator and environment are linear and passive. In addition, they have difficulty in treating uncertainty of the plant, disturbance, and noise systematically.

Another approach is to use an $\mathcal{H}_\infty$ or $\mu$-synthesis framework in which an admissible controller is designed to minimize $\mathcal{H}_\infty$ norm or $\mu$ of the closed-loop transfer function. Kazerooni *et al*. developed an $\mathcal{H}_\infty$ framework to design a controller that transmits only force signals from the master and slave robots [8]. Yan and Salcudean suggested a general framework for $\mathcal{H}_\infty$ optimization using motion scaling [9]. Leung *et al*. applied $\mu$-synthesis to design controllers for time-delayed teleoperation [10]. With these frameworks, the robust stability and robust performance of the system can be treated exactly with multiple sources of uncertainties. In the three $\mathcal{H}_\infty$ optimal approaches mentioned before, the controllers have been designed for a specific impedance of human and environment. There are also works in the teleoperation literature focusing on passivity-based design of controllers, such as for time-delayed teleoperation [11] and nonlinear teleoperation systems [12]–[15].

The proposed QC framework is to compare BTSs, which have different dynamic characteristics and sensory configurations. Since the design criterion would depend on the objective of the BTS and the environment where it is operated, the BTSs are compared with respect to a user-defined TDPO. In this paper, a $\mu$-synthesis-based formulation is used to develop the framework for the comparison of teleoperation system since $\mu$-synthesis is a well-developed method to efficiently treat systems containing uncertainties and disturbances. This is critical as BTSs suffer from the uncertainty caused by the human operator and the environment. Although some parts of $\mu$-synthesis are still open problems, we believe that it is the best tool available to treat the system with uncertainty.

As the formulation used is based on $\mu$-synthesis, which is a linear multivariable control synthesis technique, the method is directly applicable to multi-DOF manipulators, but it cannot directly handle nonlinear models. The system, operator, and environment models are represented in the form of linear nominal models with frequency-dependent multiplicative uncertainties (Section II-A).

Architectures commonly used in teleoperation systems, the performance objectives, and human and environment uncertainties in these architectures are described in Section II. The QC methodology is presented in Section III. In Section IV, the proposed methodology is applied to a case study, and a procedure to compare BTSs for the given TDPO is developed. Also, some techniques for the comparison are introduced to summarize the results. This section can be an example for readers wishing to apply the methodology for their own systems. In Section V, the proposed methodology is validated through experiments, by comparing the experimental performance of six different BTSs and four different sensory configurations with the QC analysis results. This is followed by the concluding discussions in Section VI.

## II. Formulation

The objective of this paper is the development of a methodology for systematically and quantitatively studying the effects of the master and slave manipulator mechanisms, the combination of sensors and actuators used, and their dynamic and noise properties, subject to specified task and TDPO. The formulation that will be used for specifying the system, task, human operator and environment characteristics, and performance objectives will be based on the robust control methodology of modern systems theory. Therefore, the expressive capabilities of the robust control design framework to model and incorporate uncertainties will be inherited. We will specifically include in the formulation the uncertainties in the dynamic models of the mechanisms, human operator, and environment, as well as the system disturbances originating from sensor noise and quantization effects. Also, as the robust control methodology is immediately applicable to multi-input–multi-output systems, it will be possible to seamlessly model and study multi-DOF teleoperation systems without any special treatment. In the following sections, the formulation that will be used in the subsequent analysis will be introduced, presenting the BTS model in Section II-A, human operator and environment models in Section II-B, and performance objective that will be used in Section II-C.

### A. Model of the BTS

In this study, we will assume a linear manipulator model with structured multiplicative dynamic uncertainty with additive disturbance [16], which can be represented in the form of linear fractional transformation (LFT), as shown in Fig. 1

The manipulator models with multiplicative uncertainty are as follows:

$$\boldsymbol{P}_m \subset \hat{\boldsymbol{P}}_m(\boldsymbol{I}+\boldsymbol{\Delta}_{pm}) = \hat{\boldsymbol{P}}_m(\boldsymbol{I}+\boldsymbol{W}_{pm}\hat{\boldsymbol{\Delta}}_{pm}) \quad (1)$$

$$\boldsymbol{P}_s \subset \hat{\boldsymbol{P}}_s(\boldsymbol{I}+\boldsymbol{\Delta}_{ps}) = \hat{\boldsymbol{P}}_s(\boldsymbol{I}+\boldsymbol{W}_{ps}\hat{\boldsymbol{\Delta}}_{ps}) \quad (2)$$

where $\boldsymbol{P}_m$ and $\boldsymbol{P}_s$ are, respectively, the master device and slave manipulator transfer functions from force input to position output, $\hat{(\cdot)}$ denotes the nominal model, and $\boldsymbol{\Delta}_{(\cdot)} \subset \mathcal{C}^{n\times n}$ denotes the multiplicative uncertainty. On the right-hand side of (1) and (2), the uncertainty term $\boldsymbol{\Delta}_{(\cdot)}$ is decomposed into $\boldsymbol{W}_{(\cdot)}$ and

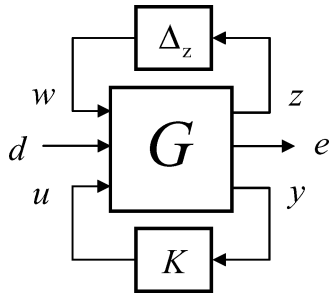


Fig. 1. LFT form representation of systems with uncertainty and disturbances. $G$: system model; $K$: controller; $\Delta_z$: uncertainty block; inputs $w, d$ and $u$: uncertainty block output, disturbance input, and control input, respectively; outputs $z$, $e$, and $y$: uncertainty block input, error signal to be minimized, and plant output, respectively.

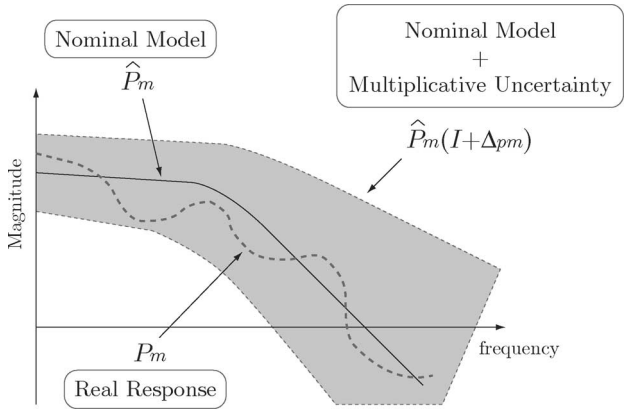


Fig. 2. Bode plot of real response and response of nominal model + uncertainty.

$\hat{\mathbf{\Delta}}_{(\cdot)} \in \boldsymbol{B}_{\mathbf{\Delta}}$, such that $\boldsymbol{B}_{\mathbf{\Delta}} = \{\Delta \in \mathbf{\Delta} : \bar{\sigma}(\Delta) \leq 1\}$.[1] Fig. 2 shows the relations of responses of the real plant, the nominal model, and uncertainty of the manipulator model in (1).

The representation of uncertainty in this form can be used to model more general perturbations (e.g., time varying, infinite dimensional, nonlinear, which may even actually be certain) provided that they are given appropriate "conic sector" interpretations via Parseval's theorem [16]–[19].

For example, LFT representations can be constructed for memoryless nonlinearities bounded by conic limits (e.g., see [20] and [21]). For more general nonlinearities, the existence of conic sector bounds can be guaranteed if the nonlinearities satisfy the Lipschitz condition, and the control and state spaces are restricted to a prescribed compact subset [22]. The nonlinear system can then be characterized as an uncertain linear system using conic sector bounds. It is important to note that the LFT representation of nonlinear systems using conic sector interpretation is an approximation. As it may be possible to quite accurately model a nonlinear element, such as quantization, rather than representing it in the form of an uncertain linear element, the LFT representation may lead to conservative results. However, the analysis techniques we use cannot directly deal with the nonlinearity, and robust control techniques in the nonlinear

[1] $\bar{\sigma}(\cdot)$ denotes the maximum singular value of $(\cdot)$.

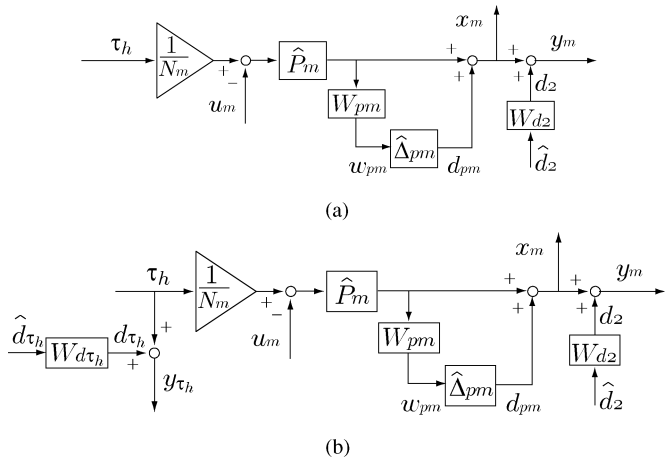


Fig. 3. Manipulator models with uncertainty and disturbance terms for two commonly used manipulator configurations. (a) Manipulator configuration with only position sensor. (b) Manipulator configuration with both position and force sensors. See Table I and Sections II and III for the details of the notation.

domain are not as comprehensive as their linear counterparts. Therefore, in this study, we chose not to pursue a nonlinear analysis, *per se*.

Fig. 3 shows the models for two commonly used manipulator configurations as examples. Fig. 3(a) shows a manipulator configuration with only a position sensor, and Fig. 3(b) shows a manipulator configuration with both position and force sensors. Gear ratio of the actuator system is explicitly included, as this is a commonly used design variable. Both of the models include the effects of the manipulator mechanism uncertainties, which can be used to model the common nonlinear effects, such as friction and backlash. The models also include the sensor noise and quantization effects modeled in the form of additive disturbance terms. In the analysis, these disturbance terms will be represented in the form

$$\boldsymbol{d}_{(\cdot)} = \boldsymbol{W}_{\boldsymbol{d}_{(\cdot)}} \hat{\boldsymbol{d}}_{(\cdot)} \tag{3}$$

where $\hat{\boldsymbol{d}}_{(\cdot)}$ is a unit random input, shaped by the frequency-dependent weight $\boldsymbol{W}_{\mathbf{d}_{(\cdot)}}$. The magnitudes of the disturbance terms (i.e., noise and quantization) are typically determined from the specifications of the sensor and data acquisition systems used. The magnitudes of the uncertainty terms resulting from the nonlinear effects are typically estimated empirically using numerical techniques. (For example, see Section IV andV).

### B. Model of the Human Operator and Environment

While most common robotic systems are designed not to be affected by dynamic interaction with the environment, communication of interaction between the human and the environment is the goal of a BTS. Therefore, human operator and environment models need to be included as part of the overall system model.

Even though a number of researchers have proposed models for human impedance (e.g., [23]), it is difficult to construct precise models since the human muscular and neural systems are

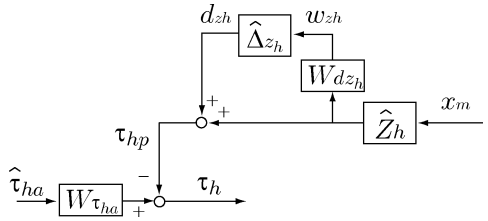


Fig. 4. Human operator model.

highly nonlinear and adaptive. The environment dynamics are usually nonlinear, uncertain, and sometimes, time varying. In this study, we will use the linear model with structured multiplicative dynamic uncertainty representation described earlier (Section II-A) to model human operator and environment dynamics:

$$\boldsymbol{Z}_h \subset \hat{\boldsymbol{Z}}_h(\boldsymbol{I}+\boldsymbol{\Delta}_{zh}) = \hat{\boldsymbol{Z}}_h(\boldsymbol{I}+\boldsymbol{W}_{zh}\hat{\boldsymbol{\Delta}}_{zh}) \tag{4}$$

$$\boldsymbol{Z}_e \subset \hat{\boldsymbol{Z}}_e(\boldsymbol{I}+\boldsymbol{\Delta}_{ze}) = \hat{\boldsymbol{Z}}_e(\boldsymbol{I}+\mathbf{W}_{ze}\hat{\boldsymbol{\Delta}}_{ze}) \tag{5}$$

where $\boldsymbol{Z}_h$, and $\boldsymbol{Z}_e$ are the human operator and environment impedances. Again, on the right-hand side of (4) and (5), the uncertainty term $\boldsymbol{\Delta}_{(\cdot)}$ is decomposed into $\boldsymbol{W}_{(\cdot)}$ and $\hat{\boldsymbol{\Delta}}_{(\cdot)} \in \boldsymbol{B}_{\boldsymbol{\Delta}}$, such that $\boldsymbol{B}_{\boldsymbol{\Delta}} = \{\Delta \in \boldsymbol{\Delta} : \bar{\sigma}(\Delta) \leq 1\}$.

A common choice in the teleoperation and haptics literature is to consider an extended uncertainty set composed of the set of all passive systems. This type of uncertainty sets typically result in conservative controllers as this is a very extensive uncertainty set. In this study, we will focus on uncertainty sets in the form of variations around a nominal model. The nominal models and uncertainty sets are typically determined empirically through experiments. If the environment or the human operator are not well characterized for the given task, then a large multiplicative uncertainty term can be used. If, on the contrary, the environment or the human operator impedance is well characterized for the given task, then a relatively precise nominal model and a small uncertainty set can be used, which would result in a less conservative, higher fidelity system.

In this paper, the intentional force command $\tau_{ha}$ and the reaction force $\tau_{hp}$ of the human operator are distinguished (Fig. 4). When there is movement of the master device caused by control input while the human operator just gripping the master device, i.e., $\tau_{ha} = 0$, then the reaction force generated by the human operator impedance $\mathbf{Z}_h$ is the reaction force. This term varies as a function of the passive dynamics of the arm as well as the stiffness generated by the cocontraction of the muscles. The intentional force command term $\tau_{ha}$ is the state-independent active component of the human operator force, and is modeled as an independent input term in the form

$$\tau_{ha} = \boldsymbol{W}_{\tau_{ha}}\hat{\tau}_{ha} \tag{6}$$

where $\hat{\tau}_{ha}$ is a unit random input, shaped by the frequency-dependent weight $\boldsymbol{W}_{\tau_{ha}}$.

### C. Performance Objectives

In an $\mathcal{H}_\infty$ or $\mu$ framework, cost functions represent the performance objectives for the system. In teleoperation, there are two commonly used performance objectives in the literature: force tracking and position tracking. If the interaction force between the slave manipulator and the environment is identical to the force between the master device and the human operator, and the operator's position constrained by the master is identical to the position of the slave, then it is called the "ideal" response of the teleoperation system [5], [6]. However, ideal response is not achievable with a practical system since it implies a marginally stable active system, which can easily become unstable as a result of uncertainties in the model, or quantization errors in a discrete-time implementation.

In the literature, two common force error forms have been used for quantifying force-tracking performance: 1) $\mathbf{e}_{f1} = \mathbf{u}_m - \tau_e$ (such as, in [1]–[4], [7], [9], [10]) and 2) $\mathbf{e}_{f2} = \tau_h - \tau_e$ (such as in [5], [6], [8]). If $\mathbf{u}_m = \tau_e$, corresponding to the exact tracking with respect to the first case, the human operator feels the dynamics of the master device as well as the interaction force at the slave side. This performance objective is useful since it does not require the dynamics of the master device, but it is inevitable for human operator to feel the dynamics of the master device. Moreover, when the actuator for the master device is nonback-drivable or the master device is heavy to handle, it is not useful to achieve realistic presence. For higher level of presence, control input should compensate for the dynamics of the master device so that human operator feels the interaction force at the slave side directly, i.e., $\tau_h = \tau_e$, corresponding to exact tracking with respect to the second case. However, since this form requires the dynamic model of the master device, it is difficult to be achieved if uncertainty is not handled properly. In the proposed framework, both of these performance objectives can be used as $\mu$-synthesis that can treat the uncertainty efficiently.

Position-tracking error is the difference between positions of the human and the slave manipulator expressed as

$$\mathbf{e}_p = \mathbf{x}_h - \mathbf{x}_s. \tag{7}$$

Here, we assume that human position is same as the master device's position, i.e., a rigid master. In (7), if $\mathbf{e}_p$ goes to zero, we can say that the master device constrains the human position to follow the slave manipulator's position or the slave manipulator follows the human position command.

TABLE I
SUMMARY OF THE NOTATION USED

| | |
|---|---|
| $\hat{\boldsymbol{P}}_m$, $\hat{\boldsymbol{P}}_s$ | Linear nominal model of the master and slave manipulator |
| $\boldsymbol{\Delta}_{pm}$, $\boldsymbol{\Delta}_{ps}$ | Uncertainty model of the master and slave manipulator |
| $\hat{\boldsymbol{Z}}_h$, $\hat{\boldsymbol{Z}}_e$ | Linear nominal model of human and environment |
| $\boldsymbol{\Delta}_{zh}$, $\boldsymbol{\Delta}_{ze}$ | Uncertainty model of human and environment |
| $\boldsymbol{d}_2$, $\boldsymbol{d}_4$ | Position sensor noise at the master and slave side |
| $\boldsymbol{d}_{\tau_h}$, $\boldsymbol{d}_{\tau_e}$ | Force sensor noise at the master and slave |
| $\boldsymbol{\tau}_{ha}$ | Human operator's active force command |
| $\boldsymbol{\tau}_{hp}$ | Human operator's passive force reaction ($\boldsymbol{\tau}_h = \boldsymbol{\tau}_{ha} + \boldsymbol{\tau}_{hp}$) |
| $\boldsymbol{\tau}_e$ | Reaction force from environment |
| $\boldsymbol{u}_m$, $\boldsymbol{u}_s$ | Control inputs at the master and slave |
| $\boldsymbol{x}_m$, $\boldsymbol{x}_s$ | Position of the master and slave |
| $\boldsymbol{y}_m$, $\boldsymbol{y}_s$ | Position sensor signal (position + sensor noise) |
| $\boldsymbol{y}_{\tau_h}$, $\boldsymbol{y}_{\tau_e}$ | Force sensor signal at the master and slave side |
| $\boldsymbol{N}_m$, $\boldsymbol{N}_s$ | Gear ratios of actuators at the master and slave side |

If the performance index includes only the force- and position-tracking error terms, the optimal controllers designed will result in infinitely large control actions. So, it is necessary to include penalty functions to keep the control inputs $\mathbf{u}_m$ and $\boldsymbol{u}_s$ below the actuator limits.

The complete cost function $\boldsymbol{e}$ in the linear fractional form (Fig. 1) to be used in the analysis is then

$$\boldsymbol{e} = [\, \boldsymbol{W}_1\boldsymbol{e}_f \quad \boldsymbol{W}_2\boldsymbol{e}_p \quad \boldsymbol{W}_3\boldsymbol{u}_m \quad \boldsymbol{W}_4\boldsymbol{u}_s \,]^T \tag{8}$$

where $\boldsymbol{W}_i$ $(i = 1, 2, 3, 4)$ are the frequency-dependent weighting vectors that emphasize more important frequency ranges, and scale the errors and control input limits. The weighting vector should be specified according to the task and performance objectives.

## III. QC Method

In this section, the QC method is introduced. Section III-A explains how to calculate the performance and stability margin in the $\mu$ framework. Section III-B introduces a feasibility test for TDPO. Section III-C presents the QC procedure.

### A. Performance Measure

In this formulation, reciprocal of the structured singular value of the system, including the $\mathcal{H}_\infty$ suboptimal controller designed using $\mu$-synthesis technique with the proper uncertainty and performance blocks, will be used as the quantitative index for objective comparison. The $\mu$-synthesis algorithm calculates a feasible controller that makes the closed-loop system stable for the specified uncertainty set, and makes the infinity norm of the transfer function from the disturbance input to error output less than or equal to 1. This synthesis algorithm can be embedded into an optimization algorithm by using an additional scaling variable $\beta$, as will be formally defined later. The proposed quantitative index can then be numerically calculated by finding the largest $\beta$ value that yields a feasible controller. This would quantify the best performance that can be achieved by the overall system with respect to the chosen application-based performance criteria, and can be used to objectively compare the effects of varying different components and design parameters of the haptic interface system. In the remainder of this section, we will formally define the performance measure we have just conceptually described.

For $\mathbf{M} \in \mathbf{C}^{n\times n}$, the structured singular value $\mu_{\boldsymbol{\Delta}}(\mathbf{M})$ is defined as

$$\mu_{\boldsymbol{\Delta}}(\mathbf{M}) = \frac{1}{\min\{\bar{\sigma}(\Delta) : \Delta \in \boldsymbol{\Delta}, \det(\mathbf{I} - \mathbf{M}\Delta) = 0\}} \tag{9}$$

where $\boldsymbol{\Delta}$ is a prescribed set of complex block diagonal matrices.[2] The interconnected system shown in Fig. 1 is well posed and internally stable, and the norm of the transfer function from disturbance inputs to error outputs $\|\mathcal{F}_u(\mathcal{F}_l(\boldsymbol{G}, \boldsymbol{K}), \Delta_z)\|_\infty \le 1$ for all $\Delta_z \in \boldsymbol{B}_{\boldsymbol{\Delta}}$ if and only if

$$\|\boldsymbol{T}\|_\mu = \sup_{\omega\in\mathbf{R}} \mu_\Delta(\boldsymbol{T}(j\omega)) \le 1 \tag{10}$$

[2]For brevity, we have not explicitly specified the block diagonal structures of $\Delta$ and $\boldsymbol{\Delta}$, since they can be determined from the context.

where $\boldsymbol{T} = \mathcal{F}_l(\boldsymbol{G}, \boldsymbol{K})$, $\Delta = \{\mathrm{diag}[\Delta_z, \Delta_f]\} \in \boldsymbol{B}_{\boldsymbol{\Delta}}$ with fictitious uncertainty block $\Delta_f$ introduced for calculating the robust performance[3] [16]. Here, $\Delta_z$ is a complex block diagonal matrix representing the structured uncertainty, where the block diagonal entries correspond to the uncertainty terms.

The $\mu$-synthesis algorithm tries to find a stabilizing controller $\boldsymbol{K}$ such that condition (10) is satisfied.

Let us introduce a weighting factor $\beta$ multiplying $\boldsymbol{T}$ and use the $\mu$-synthesis to find a stabilizing controller, such that

$$\|\beta\boldsymbol{T}\|_\mu = \sup_{\omega\in\mathbf{R}} \mu_\Delta(\beta\boldsymbol{T}(j\omega)) \le 1. \tag{11}$$

From (11), if $\|[\boldsymbol{w}^T, \boldsymbol{d}^T]^T\|_2 \le 1$, then $\beta\|[\boldsymbol{z}^T\boldsymbol{e}^T]^T\|_2 \le 1$, for $\Delta \in \boldsymbol{B}_{\boldsymbol{\Delta}}$. Therefore, $\|[\boldsymbol{z}^T, \boldsymbol{e}^T]^T\|_2 \le 1/\beta$. Larger $\beta$ presents more robustness, in the sense of stability, and better performance. This forms the basis of the QC methodology that is developed in the rest of this section.

The aforementioned scheme can be incorporated into an optimization scheme, finding the largest $\beta$ value ($\beta_{\max}$) such that (11) is satisfied. $1/\beta_{\max}$ quantifies the achievable performance and stability margin when $\Delta_f$, $\Delta_z \in \boldsymbol{B}_{\boldsymbol{\Delta}}$. From (8), $W_1$ is decomposed into its magnitude, $\beta_1 = \|\boldsymbol{W}_1\|_\infty$, and a unit magnitude transfer function, $\tilde{\boldsymbol{W}}_1 = \boldsymbol{W}_1/\|\boldsymbol{W}_1\|_\infty$. $\boldsymbol{W}_2$, $\boldsymbol{W}_{zh}$, and $\boldsymbol{W}_{ze}$ from (8), (4), and (5) are similarly decomposed into two parts, $\beta_2\tilde{\boldsymbol{W}}_2$, $\beta_{zh}\tilde{\boldsymbol{W}}_{zh}$, and $\beta_{ze}\tilde{\boldsymbol{W}}_{ze}$, respectively. If $\Delta_f \in \boldsymbol{B}_{\boldsymbol{\Delta}}$ and $\|\boldsymbol{e}\|_2 \le 1$ for a unit disturbance, $\|\boldsymbol{d}\|_2 \le 1$, in Fig. 1

$$\left\{ \begin{array}{l} |\beta_1| \cdot \|\tilde{\boldsymbol{W}}_1(\boldsymbol{\tau}_h - \boldsymbol{\tau}_e)\|_2 \le 1 \\ |\beta_2| \cdot \|\tilde{\boldsymbol{W}}_2(\boldsymbol{x}_m - \boldsymbol{x}_s)\|_2 \le 1 \end{array} \right\}$$

which gives

$$\|\tilde{\boldsymbol{W}}_1(\tau_h - \tau_e)\|_2 \le |\frac{1}{\beta_1}| \tag{12}$$

$$\|\tilde{\boldsymbol{W}}_2(\boldsymbol{x}_m - \boldsymbol{x}_s)\|_2 \le |\frac{1}{\beta_2}|. \tag{13}$$

Therefore, $1/\beta_1$ and $1/\beta_2$ represent the upper bounds of the force- and position-tracking errors, respectively.

Let $\Delta_z = \mathrm{diag}[\Delta_{zh}^T, \Delta_{ze}^T]^T$. If $\Delta_z \in \boldsymbol{B}_{\boldsymbol{\Delta}}$ and $\|\boldsymbol{z}\|_2 \le 1$ for unit perturbation, $\|\boldsymbol{w}\|_2 \le 1$, i.e., $\|\boldsymbol{T}_{11}\|_\infty \le 1$, the system is stable by the small gain theorem. In other words, the system is stable when

$$\|\Delta_z'\|_\infty = \left\| \left[ \begin{array}{cc} \beta_{zh} & 0 \\ 0 & \beta_{ze} \end{array} \right] \left[ \begin{array}{cc} \Delta_{zh} & 0 \\ 0 & \Delta_{ze} \end{array} \right] \right\|_\infty < \|\beta_z\|_\infty \tag{14}$$

and

$$\|\boldsymbol{z}'\|_\infty = \|[\tilde{\boldsymbol{W}}_{zh}\boldsymbol{Z}_h\boldsymbol{x}_m, \tilde{\boldsymbol{W}}_{ze}\boldsymbol{Z}_e\boldsymbol{x}_e]\|_\infty > 1/\|\beta_z\|_\infty \tag{15}$$

where $\|\beta_z\|_\infty = \|\mathrm{diag}[\beta_{zh}, \beta_{ze}]\|_\infty$. Hence, $\|\beta_z\|_\infty$ quantifies the stability margin from (14) and (15). Therefore, when $\Delta_f, \Delta_z \in \boldsymbol{B}_{\boldsymbol{\Delta}}$, error minimization can be stated as minimization of $|1/\beta_1|$ and $|1/\beta_2|$ and the stability margin maximization as minimization of $|1/\beta_{zh}|$ and $|1/\beta_{ze}|$.

[3]$\mathcal{F}_l$ and $\mathcal{F}_u$, respectively, refer to the lower and upper LFT forms [24].

TABLE II
CLASSIFICATION OF A BTS FOR TDPO

| | |
|---|---|
| Type 1 | Given TDPO is feasible.<br>Quantitative comparison is possible. |
| Type 2 | Given TDPO is not feasible.<br>TDPO becomes feasible if TDPO is relaxed. |
| Type 3 | Given TDPO is not feasible.<br>Stability of TDPO is not guaranteed. |

### *B. Feasibility Test for TDPO*

A TDPO for a BTS is specified by the choice of position and force performance objective bounds $\beta_1'$ and $\beta_2'$ and the stability margins $\beta_{zh}'$ and $\beta_{ze}'$ in (12)–(15).

As an example, consider the following situation.

1) A BTS should be robust to 20% uncertainty for nominal impedances of a human operator and environment to guarantee the stability of a BTS.
2) Force- and position-tracking errors should be less than 0.1 N and 0.5 mm to complete a given task.

Then, the desired performance and stability requirements would correspond to $\beta_1 \geq \beta_1' = 10$, $\beta_2 \geq \beta_2' = 2$, $\beta_{zh} \geq \beta_{zh}' = 0.2$, and $\beta_{ze} \geq \beta_{ze}' = 0.2$ in (12)–(15). Therefore, $\beta_1'$, $\beta_2'$, $\beta_{zh}'$, and $\beta_{ze}'$ specify the TDPO.

Before QC of BTSs, a given TDPO should be tested for feasibility, i.e., if it can be achieved at the specified minimum bounds. The feasibility can be verified by evaluating $\|\boldsymbol{T}'\|_\mu$, where $\boldsymbol{T}' = \boldsymbol{T}(\beta_1', \beta_2', \beta_{zh}', \beta_{ze}')$ is the plant model multiplied with the specified weighting factors. If $\|\boldsymbol{T}'\|_\mu > 1$ for $\Delta_f$, $\Delta_z \in \boldsymbol{B_\Delta}$, then the given TDPO is feasible and QC of BTSs can proceed. Since stability margins cannot be compromised, a given BTS can fall into one of the three categories specified in Table II with respect to a given TDPO. This can be determined by the value of $\|\boldsymbol{T}'(\beta_1, \beta_2)\|_\mu$, where $\boldsymbol{T}'(\beta_1, \beta_2) = \boldsymbol{T}(\beta_1, \beta_2, \beta_{zh}', \beta_{ze}')$, when $\beta_{zh}$ and $\beta_{ze}$ are fixed to $\beta_{zh}'$ and $\beta_{ze}'$, as shown in Fig. 5. If $\boldsymbol{T}'(\beta_1', \beta_2')\|_\mu \leq 1$, as shown in Fig. 5(a), then it is type 1, which means that the TDPO is feasible. If $\|\boldsymbol{T}'\|_\mu \geq 1$, but $\|\boldsymbol{T}'(\beta_1', \beta_2')\|_\mu \leq 1$ for some $\beta_1'$ and $\beta_2'$ that are less than $\beta_1'$ and $\beta_2'$, as shown in Fig. 5(b), then the BTS is type 2, which means that although the specified TDPO is not feasible, it can be made feasible by relaxation of performance objectives. If $\|\boldsymbol{T}'\|_\mu \geq 1$ and $\|\boldsymbol{T}'(\beta_1, \beta_2)\|_\mu$ can never be less than 1 under the stability margins of the given TDPO, as shown in Fig. 5(c), then it is type 3, which means that stability of the BTS cannot be guaranteed with the specified stability margins.

If the given TDPO is feasible, i.e., type 1, for a BTS, then the BTS can be quantitatively compared with other BTSs, as explained in Section III-C.

### *C. Comparison Procedure*

Consider the following performance measures:

$$Q_{\beta_1}(\beta_2', \beta_{zh}', \beta_{ze}') = \min\left\{\frac{1}{\beta_1} | \|\boldsymbol{T}\|_\mu \leq 1, W_1 = \beta_1 \tilde{W}_1, W_2 = \beta_2 \tilde{W}_2, W_{zh} = \beta_{zh}\tilde{W}_{zh}, W_{ze} = \beta_{ze}\tilde{W}_{ze}, \beta_2 \geq \beta_2', \beta_{zh} \geq \beta_{zh}', \beta_{ze} \geq \beta_{ze}'\right\} \tag{16}$$

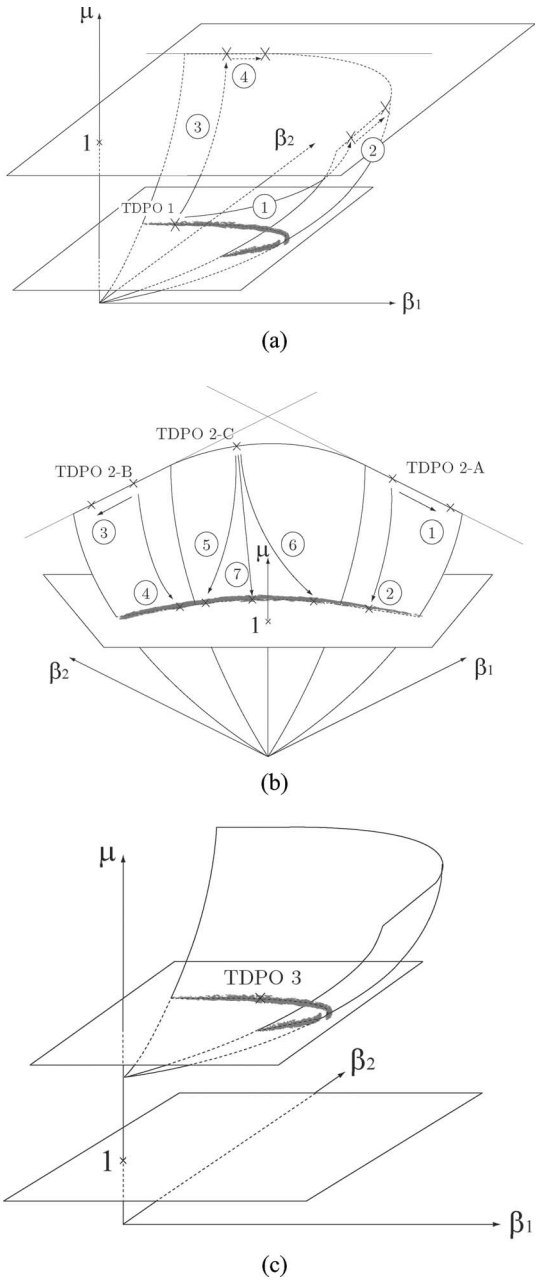


Fig. 5. Classification of TDPO. $\beta_1$ and $\beta_2$ are reciprocals of the upper bound of force- and position-tracking error in (12) and (13). (a) TDPO 1 is feasible (type 1). All combinations of $\beta_1$ and $\beta_2$ when $\mu > 1$ represent the attainable performance of the BTS. The best performance can be calculated through 1 to 2 (3 to 4) when priority of force (position)-tracking error is higher than position (force)-tracking error. (b) TDPO 2-A,B,C are unfeasible, but it can be made feasible by relaxing performance objectives (type 2). TDPO 2-A can become feasible only when force-tracking performance is relaxed as path 2. TDPO 2-B can become feasible only by relaxing position-tracking performance as path 4. TDPO 2-C can become feasible by relaxing any one of the components. (c) TDPO 3 is not feasible since the stability of a BTS is not guaranteed (type 3).

$$Q_{\beta_2}(\beta_1', \beta_{zh}', \beta_{ze}') = \min\left\{\frac{1}{\beta_2} | \|\boldsymbol{T}\|_\mu \leq 1, W_1 = \beta_1 \tilde{W}_1, W_2 = \beta_2 \tilde{W}_2, W_{zh} = \beta_{zh}\tilde{W}_{zh}, W_{ze} = \beta_{ze}\tilde{W}_{ze}, \beta_1 \geq \beta_1', \beta_{zh} \geq \beta_{zh}', \beta_{ze} \geq \beta_{ze}'\right\} \tag{17}$$

$$Q_{\beta_{zh}}(\beta_1',\beta_2',\beta_{ze}') = \min\left\{\frac{1}{\beta_{zh}} \mid\mid\mid \boldsymbol{T}\mid\mid_\mu \le 1, W_1 = \beta_1\tilde{W}_1 \right.$$
$$W_2 = \beta_2\tilde{W}_2, W_{zh} = \beta_{zh}\tilde{W}_{zh}$$
$$W_{ze} = \beta_{ze}\tilde{W}_{ze}, \beta_1 \ge \beta_1'$$
$$\left.\beta_2 \ge \beta_2', \beta_{ze} \ge \beta_{ze}'\right\} \quad (18)$$

$$Q_{\beta_{ze}}(\beta_1',\beta_2',\beta_{zh}') = \min\left\{\frac{1}{\beta_{ze}} \mid\mid\mid \boldsymbol{T}\mid\mid_\mu \le 1, W_1 = \beta_1\tilde{W}_1 \right.$$
$$W_2 = \beta_2\tilde{W}_2, W_{zh} = \beta_{zh}\tilde{W}_{zh}$$
$$W_{ze} = \beta_{ze}\tilde{W}_{ze}, \beta_1 \ge \beta_1'$$
$$\left.\beta_2 \ge \beta_2', \beta_{zh} \ge \beta_{zh}'\right\}. \quad (19)$$

In (16)–(19), $\beta_1'$, $\beta_2'$, $\beta_{zh}'$, and $\beta_{ze}'$ are the values specified for the TDPO. This comparison is performed only for the BTSs that pass the feasibility test in Section III-B. $Q_{\beta(\cdot)}$ corresponds to the limit of performance or stability margin when the other three performance objectives of the TDPO are specified among $\beta_1'$, $\beta_2'$, $\beta_{zh}'$, and $\beta_{ze}'$. Though it is more desirable to calculate a global minimization problem for $\beta_1$, $\beta_2$, $\beta_{zh}$, and $\beta_{ze}$, it does not necessarily result in a unique solution, as shown in Fig. 5(a). Therefore, we will prioritize the individual objectives in the TDPO. The best performance and stability margin can then be calculated with respect to this priority order. If the priority of force-tracking performance is higher than that of position-tracking performance, and $\beta_1'$, $\beta_2'$, $\beta_{zh}'$, and $\beta_{ze}'$ are the minimum bounds specified in TDPO, then (16)–(19) can be evaluated as

$$Q_{\beta_1}(\beta_2',\beta_{zh}',\beta_{ze}') = \frac{1}{\beta_1^*} \quad (20)$$

$$Q_{\beta_2}(\beta_1^*,\beta_{zh}',\beta_{ze}') = \frac{1}{\beta_2^*} \quad (21)$$

$$Q_{\beta_{zh}}(\beta_1^*,\beta_2^*,\beta_{ze}') = \frac{1}{\beta_{zh}^*} \quad (22)$$

$$Q_{\beta_{ze}}(\beta_1^*,\beta_2^*,\beta_{zh}^*) = \frac{1}{\beta_{ze}^*}. \quad (23)$$

The best performance and stability margin are then given as $1/\beta_1^*$, $1/\beta_2^*$, $1/\beta_{zh}^*$, and $1/\beta_{ze}^*$ for a given prioritization of the TDPO. Note that the best performance and stability will change if the priority order is changed. For example, the priorities of force tracking and position tracking are switched

$$Q_{\beta_2}(\beta_1',\beta_{zh}',\beta_{ze}') = \frac{1}{\beta_2^{**}} \le \frac{1}{\beta_2^*} \quad (24)$$

$$Q_{\beta_1}(\beta_2^*,\beta_{zh}',\beta_{ze}') = \frac{1}{\beta_1^{**}} \ge \frac{1}{\beta_1^*}. \quad (25)$$

In Fig. 5(a), paths 1 and 2 show the procedure to calculate $1/\beta_1^{**}$ and $1/\beta_2^{**}$. $1/\beta_2^{**}$ and $1/\beta_1^{**}$ are the results of paths 3 and 4.

We can summarize the procedure for our QC method as follows.

1) Specify the nominal models and uncertainties of the master, the slave, human, and environment in (1)–(5).
2) Specify the disturbance weight vectors to shape the unit random disturbances in (3), i.e., $\boldsymbol{W}_{d_2}$, $\boldsymbol{W}_{d_4}$, $\boldsymbol{W}_{\tau_{ha}}$, $\boldsymbol{W}_{d_{\tau_h}}$, and $\boldsymbol{W}_{d_{\tau_e}}$.
3) Specify the performance objectives in (8), i.e., $\boldsymbol{W}_1\boldsymbol{e}_f$ and $\boldsymbol{W}_2\boldsymbol{e}_p$.
4) Specify the control input limit in (8), i.e., $\boldsymbol{W}_3$ and $\boldsymbol{W}_4$.
5) Specify the priority of TDPO.
6) Test the feasibility.
7) If feasible, calculate QC using (16)–(19) in the specified priority order.
8) Compare the results.

We have implemented two MATLAB toolboxes for assisting interested users to apply the proposed framework for studying their systems: QC toolbox for QC for multi-DOF BTSs and simulation toolbox to verify the results of QC toolbox [25]. They are freely available for download.

## IV. Case Study

The following case study illustrates the QC method proposed in Section III. Section IV-A introduces a practical task and its prioritized TDPO. In Sections IV-B and IV-C, the comparison procedure described in Section III-C is performed and the results are discussed.

### A. Case Study Model

Consider the following task and TDPO.

1) The BTS will be used to manipulate objects made of silicon gel, which has a consistency similar to human soft tissue.
2) The operator uses his fingertip to control the master device with an input bandwidth of less than 5 Hz, which corresponds to the bandwidth of intentional hand motions.
3) Human maximum active force is less than 5 N.
4) Force- and position-tracking error should be less than 1 N under 100 Hz and 1 mm under 10 Hz, respectively.
5) BTS should be robust to the 10% and 50% of uncertainty of nominal human and environment impedance, respectively.
6) Force tracking has higher priority than that of position tracking, once the minimum performance bounds are achieved.

Table III summarizes the task and TDPO. The values for nominal impedance of human and environment are taken from [23] and [26]. $\beta_1'$, $\beta_2'$, $\beta_{zh}'$, and $\beta_{ze}'$ are calculated as shown in Section III.

The $y$-axis of PHANTOM will be used as the unit gear ratio master and slave reference models. The nominal transfer function of PHANTOM is given as follows [27], [28]:

$$P_m = P_s = \frac{1}{2.02\times10^{-5}s^2 + 6.46\times10^{-5}s}.$$

In this case study, we assume maximum actuator forces of 100 N in order to compare the teleoperation systems without considering the actuator's saturation.[4] Then,

$$W_3 = W_4 = \frac{1}{100}.$$

[4]The capability of PHANTOM actuator is actually 8.5 N. However, it is not enough to meet the given TDPO.

TABLE III
TASK AND TDPO PARAMETERS USED IN THE CASE STUDY

| | |
|---|---|
| $Z_e(s)$ | $0.35(0.05s+1)$ |
| $Z_h(s)$ | $1.51(0.05\times10^{-3}s^2+0.0219s+1)$ |
| $W_{\tau_h}$ | $5\cdot10\pi/(s+10\pi)$ |
| $\beta_1'$ | 1 |
| $\beta_2'$ | 1 |
| $\beta_{zh}'$ | 0.1 |
| $\beta_{ze}'$ | 0.5 |
| $\tilde{W}_{zh}$,$\tilde{W}_{ze}$ | 1 |
| $\tilde{W}_1$ | $200\pi/(s+200\pi)$ |
| $\tilde{W}_2$ | $20\pi/(s+20\pi)$ |

Disturbance caused by modeling error and friction are denoted by $d_1$ and $d_3$. In this case study, as disturbances, we will only consider the friction of the manipulators, neglecting the other sources of disturbance. PHANTOM has $0.04$ N end-effector friction [29]

$$W_{d_1}=W_{d_3}=0.04.$$

Sensor noises caused by quantization error in position measurement are $0.3$ mm [29]

$$W_{d_2}=W_{d_4}=0.3.$$

The amplitude of force sensor noise is assumed to be $1/40$ N, which is based on a 20 N capacity force sensor [30]

$$W_{d_{\tau_h}}=W_{d_{\tau_e}}=\frac{1}{40}.$$

As an illustration of the proposed QC method, in this case study, we will compare the effect of different sensory configurations and actuator gear ratios on the performance of a BTS. Four sensory configurations based on the placement of force sensors will be considered, namely: 1) force sensor only at the slave side (FSLAVE), 2 force sensors at both master and slave sides (FBOTH), 3) without any force sensors (FNONE), and 4) force sensor only at the master side (FMASTER).

### *B. Evaluation Methods*

Although the procedure for QC is straightforward, the large amount of data generated may make it difficult to compare BTSs since performance and stability margins are calculated for every configuration. The following procedure for each sensory configuration will be used to compare data in this case study.

1) Plot the region of each type in Table II as a function of actuator gear ratio. This shows the results of the feasibility test.
2) Plot $Q_{\beta_{(\cdot)}}(N_m,N_s)$ as a function of actuator gear ratio. This shows the results of QC.
3) Evaluate $\partial Q_{\beta_{(\cdot)}}/\partial N_m$ and $\partial Q_{\beta_{(\cdot)}}/\partial N_s$. This gives the optimal gear ratio for a BTS with respect to the specified TDPO for each sensory configuration.
4) Plot normalized $Q_{\beta_{(\cdot)}}(N_m,N_s)$ with respect to $Q_{\beta_{(\cdot)}}(N_m,N_s)$ of the architecture with force sensors on both sides (FBOTH). This shows the effect of sensory configuration.

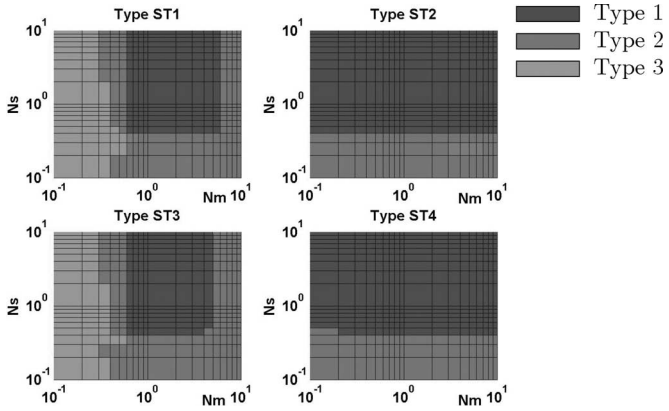


Fig. 6. Results of feasibility test with the silicon gel environment. Upper left is for architecture FSLAVE, upper right for architecture FBOTH, lower left for architecture FNONE, and lower right for architecture FMASTER, as given in Section IV-A.

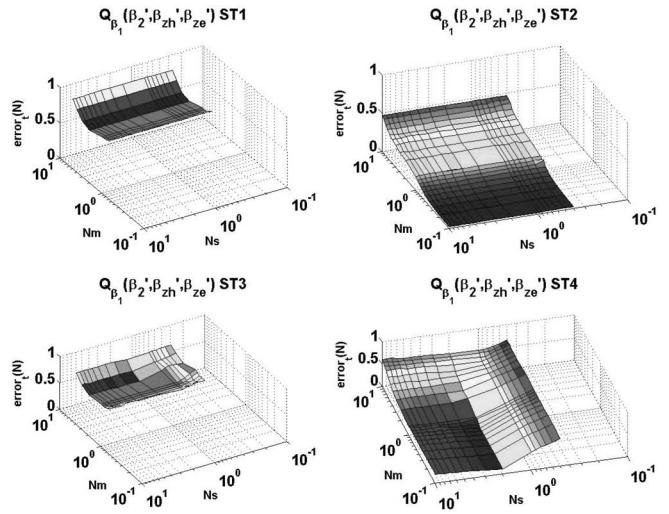


Fig. 7. $Q_{\beta_1}$ with the silicon gel environment. Upper left is for architecture FSLAVE, upper right for architecture FBOTH, lower left for architecture FNONE, and lower right for architecture FMASTER, as given in Section IV-A.

### *C. Comparison of Sensory Configuration and Drive Mechanism*

This section shows the QC results of the case study model. The results are evaluated by the procedure in Section III for BTSs with various gear ratios from $1/10$ to 10 times the nominal transfer functions $P_m$ and $P_s$ and the four kinds of sensory configurations discussed in Section IV-A.

Fig. 6 shows the results of the feasibility test of the TDPO, as described in Section III-B. For the given TDPO, the architectures that have a force sensor on the human side (FBOTH and FMASTER) are of type 1 (feasible) for gear ratios $0.4\le N_s\le 10$ and of type 2 for gear ratios $0.1\le N_s\le 0.4$ (see Section III-B). The architectures without a force sensor on the human side (FSLAVE and FNONE) are of type 1 for gear ratios $0.6\le N_m\le 6$ and $0.4\le N_s\le 10$, and of type 3, for gear ratios $0.1\le N_m\le 0.3$, and of type 2 otherwise.

For the cases that pass the feasibility test, we can proceed with the QC.

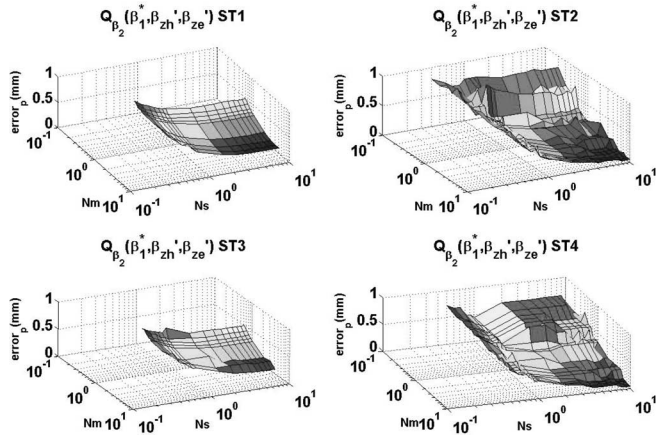


Fig. 8. $Q_{\beta_2}$ with the silicon gel environment. Upper left is for architecture FSLAVE, upper right for architecture FBOTH, lower left for architecture FNONE, and lower right for architecture FMASTER, as given in Section IV-A.

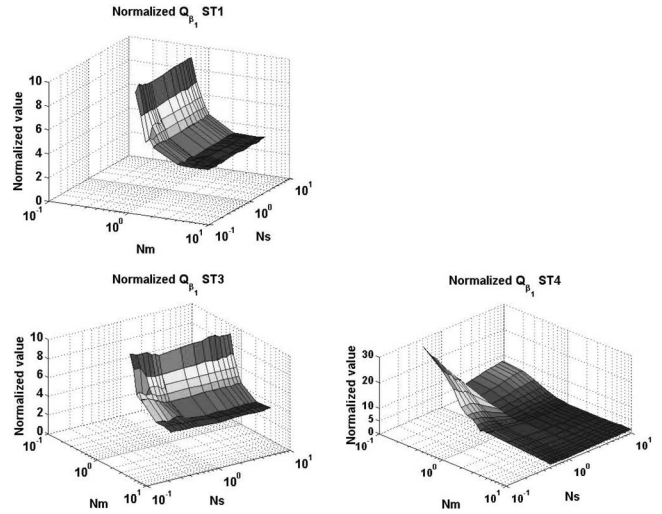


Fig. 9. Normalized $Q_{\beta_1}$ with the silicon gel environment. Upper left is for architecture FSLAVE, upper right for architecture FBOTH, lower left for architecture FNONE, and lower right for architecture FMASTER, as given in Section IV-A.

Figs. 7 and 8 show $Q_{\beta_1}(N_m, N_s)$ and $Q_{\beta_2}(N_m, N_s)$ for the four sensory configurations when the first priority is force-tracking performance. Guidelines to design a BTS for the given TDPO can be identified from the results. For example, from Fig. 7, we can conclude that the force-tracking performance of a BTS with force sensors on both sides improves with lower gear ratios on the human side, while the gear ratio on the slave side does not affect the force-tracking performance, as observed in the upper right figure. For a BTS with a force sensor on the human side, the optimal gear ratio on the slave side, $N_s = 2$, maximizes the force-tracking performance, as observed in Fig. 7(lower right). The force-tracking performance improves with lower gear ratio on the human side. From Fig. 8, we conclude that the position-tracking performance, as a second priority TDPO parameters, gets better at higher gear ratios on both human and slave sides for all BTS architectures.

Fig. 9 shows the normalized $Q_{\beta_1}(N_m, N_s)$ of each architecture with respect to the $Q_{\beta_1}(N_m, N_s)$ of the architecture that has force sensors on both sides. From the results, we can compare the performances of BTSs with various gear ratio and sensory configurations quantitatively. For example, for the best force-tracking performance, a BTS with force sensors at both sides should have gear ratio $N_m = 0.1$ and $0.4 \leq N_s \leq 10$. For that system, the achievable minimum force-tracking error will be $0.02$ N. When only one force sensor is allowed, it is more desirable to attach the sensor to the master device since that architecture has a wider region of type 1 (Fig. 6), and 10 to 100 times better force-tracking performance is guaranteed compared to the architecture with a force sensor only on the slave side. If there is a force sensor only on the slave side, the force tracking performance is not much different from that of the architecture without any force sensors, especially when $N_s > 1$ in the region of type 1. The achievable minimum force-tracking errors of the architectures with a single force sensor located on the slave and without any force sensors are 0.744 N and 0.853 N, respectively, and are achieved at $N_m = 2$ and $N_s = 4$. The achievable minimum force-tracking errors of the architecture with a force sensor only on the master side are 0.62 N, for gear ratio $N_m = 0.1$ and $N_s = 0.4$, and 0.67 N, for gear ratio $N_m = 10$ and $N_s = 0.4$. The achievable minimum force-tracking errors of the architecture with force sensors on both sides are 0.02 N, for gear ratio $N_m = 0.1$ and $N_s = 0.4$, and 0.47 N, for gear ratio $N_m = 10$ and $N_s = 0.4$. This observation suggests that the advantage of the architecture with force sensors on both sides decreases in comparison to the architecture with a force sensor only on the master side for high gear ratios of the master device, as observed in Fig. 9 (lower right). At this point, we would like to note that the observations made earlier are specific to the BTSs and TDPO considered in the analysis.

The QC method proposed in this paper can suggest guidelines to design a relevant BTS, particularly when there are constraints in choosing a sensory configuration and a drive mechanism.

## V. Experimental Validation

In this section, the validity of the proposed QC methodology is experimentally confirmed by comparing the predicted and experimentally determined performances a 2-DOF BTS tested with 24 different sensor and actuator configurations (six different actuator configurations and four different sensory configurations). The BTSs used in this experiment are described in Section V-A. The models of the BTSs and the TDPO used in the analysis are presented in Section V-C. Following these, the performances predicted using the proposed QC framework and observed through the experiments are presented and compared in Section V-D, to confirm the validity of QC framework.

### A. Experimental Setup

Two kinematically similar 2-DOF planar master and slave manipulators [Fig. 10(a) and (b)] were used in the experiments. Each of the manipulators were equipped with force/torque sensors (MINI 45, ATI Industrial Automation, Inc., Apex, NC) attached to their end points to measure the interaction forces between the human operator and the master device, and between the environment and the slave robot (Fig. 10). Using the

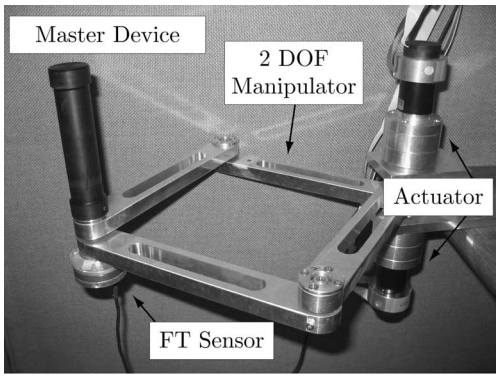


(a)

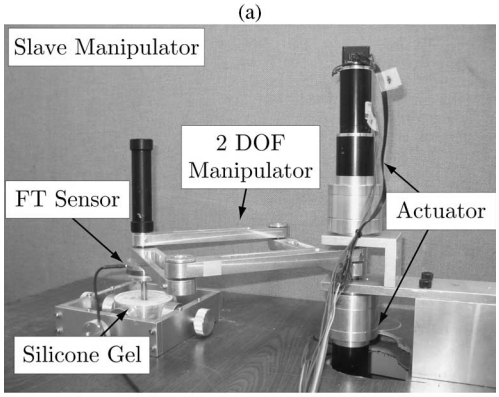


(b)

Fig. 10. (a) Two DOF master device. (b) Two DOF slave manipulator.

same mechanisms, 24 different actuator and sensor configurations, which were combinations of six actuator and four sensory configurations available, were tested. The six different actuator configurations, which are shown in Table IV, were constructed by choosing combinations of actuators for the master and slave manipulators from three available pairs of actuators. Table V shows the specifications of the actuator pairs. The actuator pairs 1, 2, and 3, respectively, consist of Maxon Co. RE 90, EC 45, and RE-max 24 DC motors, with gear heads, as shown in Table V. The backlashes of the actuators are less than $1^\circ$. At each case, the same actuator type was used for the both DOFs of a manipulator. The four sensory configurations used were distinguished based on the availability of force sensor information in the controller, where in case 1), a force sensor was only available at the slave side; in case 2), force sensors were available at both master and slave sides; in case 3), no force sensors were available; and in case 4), a force sensor was only available at the master side. In all cases, position sensors in the form of quadrature encoders were available at both master and slave sides.

A soft gel mold made from dielectric silicone gel (DSE7310, Dong Yang Silicone Company, Korea) was used to model a soft environment, which is suitable to evaluate the performance of both force tracking and position tracking, simultaneously. Soft contact tasks are rather common in medical robotics applications. The mechanical properties of this material is very close to that of human soft tissue, so as to represent an environment for a typical probing task encountered in medical robotics applications.

TABLE IV
ACTUATOR CONFIGURATIONS USED IN THE EXPERIMENTAL SETS

| Actuator pairs at master side \ Actuator pairs at slave side | 1 | 2 | 3 |
|---|---|---|---|
| 1 | | Set 3 | Set 5 |
| 2 | Set 1 | | Set 6 |
| 3 | Set 2 | Set 4 | |

TABLE V
ACTUATORS USED IN THE EXPERIMENTAL SETS

| Actuator pairs | 1 | 2 | 3 |
|---|---|---|---|
| gear ratio | 26 : 1 | 33 : 1 | 231 : 1 |
| encoder (pulse/rev.) | 2000 | 2048 | 2048 |

### *B. Experimental Task*

In the experiments conducted, the operator was instructed to perform a force following task, i.e., applying a force to the environment matching in magnitude and direction to an indicator shown on a computer screen. The force vector corresponding to the actual interaction force between the end effector and the environment, measured using a force sensor, was also shown on the screen. During the experiment, the desired force vector shown on the screen smoothly increased in magnitude from 0 N to about 4 N, while maintaining its direction. In order to keep the operator from adapting to the task, the direction of the force vector was changed randomly between trials. During the experiments, the operator was seated such that the operator's arm was aligned with $x$-axis of the master device, and was instructed to use the thumb and the index fingertips for gripping the master manipulator.

### *C. Models and TDPO Used in the QC*

In order to compare the performances of the BTSs with the six different set of actuator configurations and the four different sensory cases using the proposed QC methodology, the manipulator models in the form of linear nominal models and uncertainties were calculated. The nominal manipulator models for the different actuation cases were experimentally determined using black box system identification. It was also empirically determined that the uncertainty margin of the master and slave manipulator is $20\%$ under 5 Hz and $40\%$ above 10 Hz, i.e.,

$$\Delta_{pm} = \Delta_{ps} = 0.2\left(\frac{1}{10\pi}s + 1\right)\left(\frac{1}{20\pi}s + 1\right) \tag{26}$$

nominal models and uncertainties can represent real nonlinear manipulators including actuator pairs of experimental sets.

Similarly, the nominal model and uncertainty margins for human operator and environment were also experimentally determined using black box system identification using a technique similar to that in [8]. The $x$-axis and $y$-axis nominal models of human and environment used are given in Table VI. A $50\%$ uncertainty margin over the whole frequency range was determined to cover the real nonlinear human operator and environment; therefore, $\Delta_{zh} = \Delta_{ze} = 0.5$. For the task in this

TABLE VI
LINEAR NOMINAL MODELS OF HUMAN OPERATOR AND ENVIRONMENT USED IN THE EXPERIMENTAL SETS

| Human and Env. | Transfer function of linear nominal model |
|---|---|
| x-axis of human | $\frac{0.0163s^2+0.4867s+66.1484}{s^2+20.0001s+118.0289}$ |
| y-axis of human | $\frac{0.0035s^2+0.9652s+47.0628}{s^2+10.6649s+46.6923}$ |
| x-axis of env. | $\frac{0.0127s^2+0.6274s+57.2645}{s^2+11.1362s+59.9781}$ |
| y-axis of env. | $\frac{0.0018s^2+1.2663s+52.9774}{s^2+6.2843s+23.4865}$ |

experiment, the human active force is assumed to be less than 5 N and under 3 Hz.

The following performance objective functions were used to define the TDPO for these experimental sets. In this experiment, the force-tracking performance has higher priority than that of the position tracking, as the subjects are asked to perform a force-tracking task. The minimum performance for force tracking and position tracking were chosen as 5 N under 5 Hz and 5 mm under 5 Hz, respectively. In order to compare the experimental sets fairly, the control input was constrained by 10 N under 5 Hz and 0.1 N above 50 Hz at the gear end. The resulting TDPO for performance output can be represented as follows:

$$\boldsymbol{W}_1 = 0.2\begin{bmatrix} \frac{1000\pi^3}{(s+10\pi)^3} & 0 \\ 0 & \frac{1000\pi^3}{(s+10\pi)^3} \end{bmatrix} \tag{27}$$

$$\boldsymbol{W}_2 = 0.2\begin{bmatrix} \frac{1000\pi^3}{(s+10\pi)^3} & 0 \\ 0 & \frac{1000\pi^3}{(s+10\pi)^3} \end{bmatrix} \tag{28}$$

$$\boldsymbol{W}_3 = 0.1N_m\begin{bmatrix} \frac{(1/100\pi s+1)^3}{(1/10\pi s+1)^3} & 0 \\ 0 & \frac{(1/100\pi s+1)^3}{(1/10\pi s+1)^3} \end{bmatrix} \tag{29}$$

$$\boldsymbol{W}_4 = 0.1N_s\begin{bmatrix} \frac{(1/100\pi s+1)^3}{(1/10\pi s+1)^3} & 0 \\ 0 & \frac{(1/100\pi s+1)^3}{(1/100\pi s+1)^3} \end{bmatrix} \tag{30}$$

In this experiment, force sensor noise and position sensor noise will be represented as disturbances with magnitude 0.25 N and 1 mm over the whole frequency range, i.e., $\mathbf{d}_{th} = \mathbf{d}_{te} = [0.25 \quad 0.25]^T$ and $\mathbf{d}_2 = \mathbf{d}_4 = [0.001 \quad 0.001]^T$.

### D. QC Results Compared With the Experimental Results

The goal of the experiment was to confirm the validity of the proposed QC framework through a comparison of QC results and experimental results. In the previous section, the linear models, uncertainties, and TDPOs for 24 experimental sets were described. Using the QC framework via the developed QC MATLAB toolbox, the QC results were calculated for the various sensory configurations and experimental sets. As described in Section III, the proposed QC method has two main steps: testing the feasibility of a given TDPO and evaluating the performance measures. The experiments were performed using controllers obtained by model reduction from the $\mathcal{H}_\infty$ suboptimal controllers generated by the $\mu$-synthesis algorithm used in the second step of the QC.

At this point, it is important to note that the results of the QC and the experiments can be compared only indirectly. The QC calculations optimize the worst case performance of the system under the specified uncertainties and disturbances. As an exhaustive experiment that tests all possible human operator, environment, and system uncertainties, and user inputs is not possible, the experiments can only test specific instances. The experimental results reported are the tracking performance of each of the systems, calculated as the ratio of the $L_2$ norms of the tracking error and user input forces, for those specific instances of the user input, human operator, environment, and other uncertainties, etc., captured in the experiments. Therefore, the performance values given by the QC analysis are expected to be the upper bounds of the actual tracking error values of the system observed during the experiments.

Figs. 11 and 12 show the results of the QC and the experiments. The experimental force and position tracking errors are less than the performance values predicted by QC analysis, as expected. Furthermore, the performance trends observed from the experimental results match those predicted by the QC analysis. Therefore, the experimental results validate the proposed QC method.

## VI. CONCLUDING REMARKS

In this paper, we have proposed a quantitative method to evaluate teleoperation system based on a given TDPO, using $\mu$-synthesis. Our approach is distinguished from the previous works in the literature as our focus is to evaluate and guide the design of the overall system, not just to design a controller for a given system. In order to compare BTSs quantitatively, we employ a TDPO. Using $\mu$-framework, performance and stability margin, which form the TDPO, can be evaluated quantitatively while modeling uncertainties and noise. From the result, we can compare BTSs quantitatively, and quantitative design guidelines can be determined, which optimize the BTS for the given TDPO.

The most important benefit of the proposed framework is that it makes possible the design of a BTS considering its task and environment from a systems point of view. It can be used effectively as a design guideline when there are constraints in choosing drive mechanisms and the sensory configuration for a BTS, especially the one designed to be operated in constrained conditions.

It is interesting to note that the design choices that would be based on the results of the QC would be potentially different from those that would be based on the results of a limited set of experiments, such as those reported in Section V, as it is not feasible to perform an exhaustive set of experiments covering all the possible cases of inputs, environments, operators, etc. A design based on such a limited set of experiments would, by no means, be optimal, and could potentially lead to pitfalls. This is actually one of the main reasons behind developing an analytical and quantitative design framework, such as the one we have proposed here.

The tradeoff between system performance and uncertainty in the system is a fundamental constraint in the design of control systems. Instead of always using an infinitely large uncertainty term (corresponding to all possible passive human operators

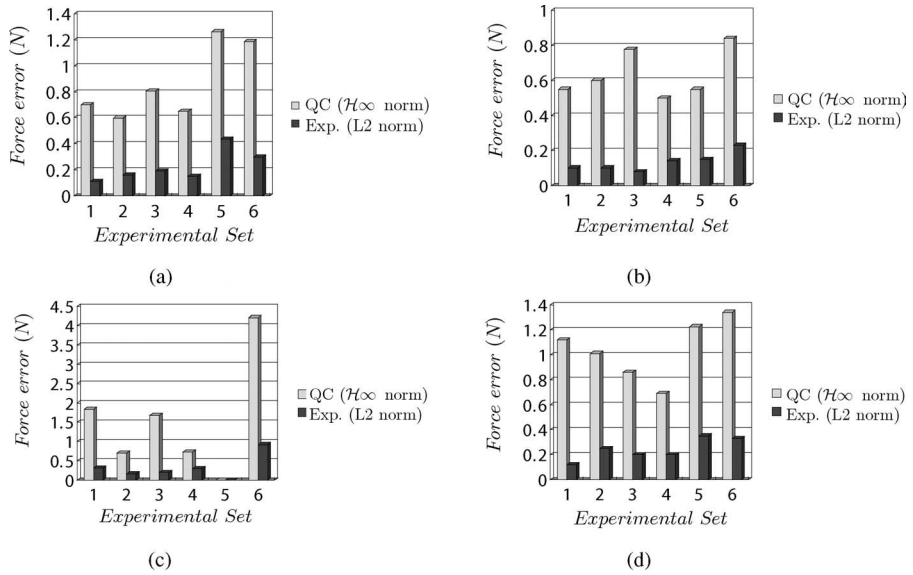


Fig. 11. Force-tracking errors predicted by the QC framework and observed in the experiments. (a) Sensory configuration (FSLAVE). (b) Sensory configuration (FBOTH). (c) Sensory configuration (FNONE). (d) Sensory configuration (FMASTER). QC results are the predicted $\mathcal{H}_\infty$ norms of the transfer functions from the user inputs to tracking error outputs. The experimental results are the ratios of the $L_2$ norms of the tracking errors and user input forces.

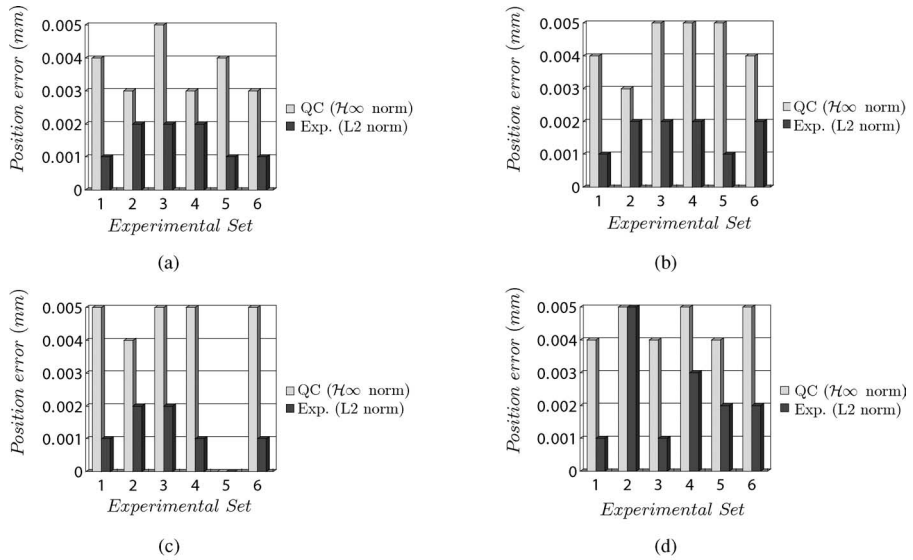


Fig. 12. Position-tracking error predicted by the QC framework and observed in the experiments for each experimental set. (a) Sensory configuration (FSLAVE). (b) Sensory configuration (FBOTH). (c) Sensory configuration (FNONE). (d) Sensory configuration (FMASTER).

and environments), in the proposed approach, it is possible to explicitly select the size of the uncertainty terms, ranging from no uncertainty, to all passive systems, and in between, based on the specific task under consideration. This provides an important flexibility in the analysis.

At this point, it would be informative to note the differences between the QC methodology developed in this paper and the approach proposed by the coauthor Çavuşoğlu in [7]. Although the goal of the two papers are similar, the basic formulation, the way the uncertainties are modeled, the quantitative performance measure used, the TDPOs used, and the overall comparison method are all different between the two approaches. Table VII summarizes the differences between the two approaches. Specifically, the formulation and the QC method presented in the current manuscript are significantly more extensive in scope in terms of expressive capabilities and the design variables that can be analyzed.

Time delay is one of the important issues for teleoperation systems. The constant time delay case has already been treated through $\mu$-synthesis by Leung *et al.* [10]. We have not specifically focused on time delay effects in our presentation, as Leung *et al.*'s method can be applied to our methodology if evaluation of time delay effects is desired. Time-varying delay and data loss in the communication channel are major unsolved problems in the field of teleoperation, and therefore, outside the scope of our paper.

An interesting QC case is the evaluation of BTSs in tasks that involve contact with rigid environments. In such a case,

TABLE VII
COMPARISON OF THE QC METHOD DEVELOPED IN THIS PAPER AND THE APPROACH PROPOSED IN [7]

| | QC approach proposed in [7] | QC method developed here |
|---|---|---|
| Basic formulation | $H_\infty$ | $\mu$-synthesis |
| Uncertainty model | Lumped unstructured uncertainty | Structured uncertainty |
| Quantitative performance measure | $H_\infty$ norm of the performance objective functional | Reciprocal of the structured singular value of the system |
| Task dependent performance objective used | Single quantitative measure. | Prioritized requirements on force and position tracking, and actuator output limitations. |
| Overall comparison algorithm | Fidelity alpha curve constructed using a constrained optimization, with constraints on stability and position tracking, with an assumed controller structure | Comparison algorithm is based on an unconstrained optimization, with a separate feasibility test for stability and minimal performance. No controller structure is assumed a priori. |

if desired, the transition behavior can be modeled using the proposed uncertainty formulation using an uncertainty bound ranging from free space to constrained space (which may go to infinity if infinitely rigid contact is considered). However, this is not necessarily an effective method of evaluating a BTS design. Specifically, the proposed QC method uses, in determining the performance of the system, a *single* $H_\infty$ suboptimal controller designed using the whole uncertainty set specified. However, in practical application involving such contact tasks, a switching control strategy is typically used for separately handling free space, contact transition, and contact cases. Therefore, a better comparison strategy would be to consider each of these cases separately, each of which would then have a smaller uncertainty set.

## REFERENCES


[1] B. Hannaford, "A design framework for teleoperators with kinesthetic feedback," *IEEE Trans. Robot. Autom.*, vol. 5, no. 4, pp. 426–434, Aug. 1989.

[2] R. J. Anderson and M. W. Spong, "Bilateral control of teleoperators with time delay," *IEEE Trans. Autom. Control*, vol. 34, no. 5, pp. 494–501, May 1989.

[3] J. E. Colgate and J. M. Brown, "Factors affecting the z-width of a haptic display," in *Proc. IEEE Int. Conf. Robot. Autom.*, May 1994, pp. 3205–3210.

[4] R. J. Adams and B. Hannaford, "Stable haptic interaction with virtual environment," *IEEE Trans. Robot. Autom.*, vol. 15, no. 3, pp. 465–474, Jun. 1999.

[5] D. A. Lawrence, "Stability and transparency in bilateral teleoperation," *IEEE Trans. Robot. Autom.*, vol. 9, no. 5, pp. 624–637, Oct. 1993.

[6] Y. Yokokohji and T. Yoshikawa, "Bilateral control of master–slave manipulators for ideal kinesthetic coupligng-formulation and experiment," *IEEE Trans. Robot. Autom.*, vol. 10, no. 5, pp. 605–620, Oct. 1994.

[7] M. C. Çavuşoğlu, A. Sherman, and F. Tendick, "Design of bilateral teleoperation controllers for haptic exploration and tele manipulation of soft environment," *IEEE Trans. Robot. Autom.*, vol. 18, no. 4, pp. 641–647, Aug. 2002.

[8] H. Kazerooni, T. Tsay, and K. Hollerbach, "A controller design framework for telerobotic systems," *IEEE Trans. Control Syst. Technol.*, vol. 1, no. 1, pp. 50–62, Mar. 1993.

[9] J. Yan and S. E. Salcudean, "Teleoperation controller design using $\mathcal{H}_\infty$ optimization with application to motion-scaling," *IEEE Trans. Control Syst. Technol.*, vol. 4, no. 3, pp. 244–258, May 1996.

[10] G. M. H. Leung, B. A. Francis, and J. Apkarian, "Bilateral controller for teleoperators with time delay via $\mu$-synthesis," *IEEE Trans. Robot. Autom.*, vol. 11, no. 1, pp. 105–116, Feb. 1995.

[11] G. Niemeyer and J. J. E. Slotine, "Stable adaptive teleoperation," *IEEE J. Ocean. Eng.*, vol. 16, no. 1, pp. 152–162, Jan. 1991.

[12] K. Kosuge, T. Itoh, and T. Fukuda, "Human–machine cooperative telemanipulation with motion and force scaling using task-oriented virtual tool dynamics," *IEEE Trans. Robot. Autom.*, vol. 16, no. 5, pp. 505–516, Oct. 2000.

[13] N. V. Q. Hung, T. Narikiyo, and H. D. Tuan, "Nonlinear adaptive control of master–slave system in teleoperation," *Control Eng. Pratice*, vol. 11, no. 1, pp. 1–10, 2003.

[14] D. J. Lee and P. Y. Li, "Passive tool dynamics rendering for nonlinear bilateral teleoperated manipulators," in *Proc. IEEE Int. Conf. Robot. Autom.*, 2002, pp. 3284–3289.

[15] D. J. Lee and P. Y. Li, "Passive coordination control to nonlinear bilateral teleoperated manipulators," in *Proc. IEEE Int. Conf. Robot. Autom.*, 2002, pp. 3278–3283.

[16] K. Zhou, J. C. Doyle, and K. Glover, *Robust and Optimal Control*. Englewood Cliffs, NJ: Prentice-Hall, 1996.

[17] G. Zames, "On the input–output stability of nonlinear time-varying feedback systems, Part I," *IEEE Trans. Autom. Control*, vol. AC-11, no. 2, pp. 228–238, Apr. 1966.

[18] G. Zames, "On the input–output stability of nonlinear time-varying feedback systems, Part II," *IEEE Trans. Autom. Control*, vol. AC-11, no. 3, pp. 465–476, Jul. 1966.

[19] M. G. Safonov, *Stability and Robustness of Multivariable Feedback Systems*. Cambridge, MA: MIT Press, 1980.

[20] R. D. Braatz and M. Morari, "Stability and performance analysis of systems under constraints," Control Dyn. Syst., Calif. Inst. Technol., Tech. Rep., Tech. Memorandum No. CIT-CDS 93-009, 1993.

[21] M. Kothare, P. J. Campo, M. Morari, and C. N. Nett, "A unified framework for the study of anti-windup designs," Control Dyn. Syst., Calif. Inst. Technol., Tech. Rep., Memor. CIT-CDS 93-011, 1993.

[22] C.-P. Chao and P. M. Fitzsimons, "Stabilization of a large class of nonlinear systems using conic sector bounds," *Automatica*, vol. 33, no. 5, pp. 945–953, Jan. 1997.

[23] P. Buttolo, "Characterization of human pen grasp with haptic displays," Ph.D. dissertation, Dept. Electr. Eng., Univ. Washington, Seattle, 1996.

[24] K. Zhou and J. C. Doyle, *Essentials of Robust Control*. Englewood Cliffs, NJ: Prentice-Hall, 1998.

[25] K. Kim, M. C. Çavuşoğlu, and W. K. Chung. (2006). Matlab toolbox for quantitative comparison of teleoperation systems [Online]. Available: http://robotics.case.edu/QCToolbox/

[26] A. Sherman, M. C. Çavuşoğlu, and F. Tendick, "Comparison of teleoperator control architectures for palpation task," in *Proc. ASME Dyn. Syst. Control Division, Part ASME Int. Mech. Eng. Congr. Expo. (IMECE 2000)* Nov., pp. 1261–1268

[27] M. C. Çavuşoğlu, D. Feygin, and F. Tendik, "A critical study of the mechanical and electrical properties of the phantom haptic interface and improvement for high performance control," *Presence*, vol. 11, no. 6, pp. 555–568, 2002.

[28] M. C. Çavuşoğlu and F. Tendick, "Kalman filter analysis for quantitative comparison of sensory schemes in bilateral teleoperation systems," in *Proc. IEEE Int. Conf. Robot. Autom.*, Taipei, Taiwan, Sep. 2003, pp. 2818–2823.

[29] The Sensable Technology, Inc., [Online]. Available: http://www.sensable.com Jun. 21 2007

[30] Ati Force Sensor, Inc., [Online]. Available: http://www.ati-ia.com Jun. 21 2007



**Keehoon Kim** (M'05–AM'07) received the B.S., M.S., and Ph.D. degrees in mechanical engineering from Pohang University of Science and Technology (POSTECH), Pohang, Korea, in 1999, 2001, and 2006, respectively.

From Fall 2003 to Spring 2004, he was a visiting student at the Case Western Reserve University, Cleveland, OH. He is currently a Postdoctoral Researcher in the Department of Mechanical Engineering, Northwestern University, Evanston, IL. His current research interests include design of bilateral teleoperation systems and haptic/tactile devices, surgical robotics, and robust controllers for haptic interfaces.

**M. Cenk Çavuşoğlu** (S'93–M'01–SM'06) received the B.S. degree in electrical and electronic engineering from the Middle East Technical University, Ankara, Turkey, in 1995, and the M.S. and Ph.D. degrees in electrical engineering and computer sciences from the University of California, Berkeley, in 1997 and 2000.

From 2000 to 2002, he was a Postdoctoral Researcher and a Lecturer in the Department of Electrical Engineering and Computer Sciences, University of California. He is currently an Assistant Professor of electrical engineering and computer science at the Case Western Reserve University, Cleveland, OH. His current research interests include robotics (medical robotics and haptics), virtual environments and computer graphics (surgical simulation and physical modeling), and systems and control theory.

Dr. Çavuşoğlu is as an Associate Editor of the IEEE TRANSACTIONS ON ROBOTICS.

**Wan Kyun Chung** (S'84–M'86) received the B.S. degree in mechanical design from Seoul National University, Seoul, Korea, in 1981, and the M.S. degree in mechanical engineering and the Ph.D. degree in production engineering from Korea Advanced Institute of Science and Technology (KAIST), Seoul, in 1983 and 1987, respectively.

During 1988, he was a Visiting Professor at the Robotics Institute, Carnegie-Mellon University, Pittsburgh, PA, and during 1995, he was a Visiting Scholar at the University of California, Berkeley. He is currently a Professor in the Department of Mechanical Engineering, Pohang University of Science and Technology (POSTECH), Pohang, Korea, where he has been a Faculty Member since 1987. His current research interests include localization and navigation for mobile robots, underwater robots, and bio-robots.

Prof. Chung is an Associate Editor for several journals including the IEEE TRANSACTIONS ON ROBOTICS. He is also the Director of the National Research Laboratory for Intelligent Mobile Robot Navigation.